# Powered Knee and Ankle Prosthesis Control for Adaptive Ambulation at Variable Speeds, Inclines, and Uneven Terrains

Liam M. Sullivan, Suzi Creveling, Marissa Cowan, Lukas Gabert, and Tommaso Lenzi, Member, IEEE

Abstract— Ambulation in everyday life requires walking at variable speeds, variable inclines, and variable terrains. Powered prostheses aim to provide this adaptability through control of the actuated joints. Some powered prosthesis controllers can adapt to discrete changes in speed and incline but require manual tuning to determine the control parameters, leading to poor clinical viability. Other data-driven controllers can continuously adapt to changes in speed and incline but do so by imposing the same non-amputee gait patterns for all amputee subjects, which does not consider subjective preferences and differing clinical needs of users. Here, we present a controller for powered knee and ankle prostheses that can continuously adapt to different walking speeds, inclines, and uneven terrains without enforcing a specific prosthesis position, impedance, or torque. A virtual biarticular muscle connection determines the knee flexion torque, which changes with both speed and slope. Adaptation to inclines and uneven terrains is based solely on the global shank orientation. Continuously variable damping allows for speed adaptation. Minimum-jerk programming defines the prosthesis swing trajectory at variable cadences. Experiments with one individual with an above-knee amputation suggest that the proposed controller can effectively adapt to different walking speeds, inclines, and rough terrains.

## I. INTRODUCTION

Ambulation with conventional passive prostheses is slow and inefficient, resulting in poor mobility and quality of life for individuals with lower-limb amputations [1]. Powered prostheses have the potential to address this problem by closely matching the torque, speed, and power capabilities of biological legs [2]–[5]. However, the clinical viability of powered prostheses is limited by the ability of available controllers to adapt to the variability of the real world.

Powered prosthesis controllers aim to imitate the biomechanical function of the human leg during ambulation. To this end, most controllers assume that the ambulation task is periodic and break down the gait cycle into a discrete number of phases [2], [6] or a continuous phase evolution [7], [8], often using finite-state machines [9]. Based on the online estimate of the discrete or continuous gait phase, the controller defines a desired torque [6], [10], impedance [9], [11], or position [9], [11] of the powered prosthesis joint. The specific values of the torque, impedance, and position for each gait phase can be manually tuned by the experimenter [12] or automatically selected based on non-amputee datasets [10]. This approach attempts to imitate the function of the intact human leg at different walking speeds, cadences, and terrain inclines, which can be estimated online using the sensors embedded in the prosthesis.

\*Research supported by the National Institutes of Health under grant number R01 HD098154/HD/NICHD, the National Institute for Occupational Safety and Health under Grant T42/CCT810426, and the US Department of Defense under Grant W81XWH2110037. All authors are currently affiliated with the Department of Mechanical Engineering and Robotics Center at the

Controllers that rely on manual tuning of the impedance settings during each discrete gait phase adapt to changes in speed and incline by defining behavior between discrete thresholds (e.g., -10°, 0°, 10° incline, slow, normal, fast speed) [13]. This approach works well, but only close to the thresholds. Increasing the number of thresholds can improve function but is not clinically viable due to the time needed to manually determine the control parameters between each threshold and during each gait phase.

Some prosthesis controllers can continuously adapt to changes in speed [10] or incline [14], [15]. These controllers do not require manual tuning because they are based on data recorded from non-amputee subjects ambulating at different speeds and inclines. Continuous adaptation more accurately matches able-bodied kinematics and kinetics compared to discrete adaptation and does not require subject-specific tuning [14]. However, purely data-driven approaches require large datasets, including every possible combination of speed, incline, terrain roughness, and compliance. Moreover, a purely data-driven approach imposes the same gait pattern for all subjects. Therefore, it does not consider personal preference or other important factors such as the length of the residual limb, strength of the user, or sound-limb functionality.

Control based on invariant behaviors in non-amputee biomechanics is an alternative approach to achieving continuous adaptation without enforcing a specific gait pattern. For example, minimum-jerk programming allows for continuous adaptation to speed, cadence, and clearance in swing without imposing a predefined trajectory [11]. Similarly, using the global orientation of the shank in impedance controllers allows for continuous adaptation to different inclines, and even to rough terrains, in below-knee prostheses [15]. Invariant gait behaviors could lead to speed and incline adaptive controllers for powered prostheses.

In this paper, we present a controller for powered knee and ankle prostheses that can continuously adapt to different walking speeds, inclines, and uneven terrains. The proposed controller is inspired by invariant non-amputee biomechanics and does not enforce a specific prosthesis position, impedance, or torque. A virtual biarticular muscle connection determines the knee flexion torque. Adaptation to inclines and uneven terrains is based solely on the global shank orientation. Continuously variable damping allows for speed adaptation. Minimum-jerk programming defines the prosthesis swing trajectory at variable speeds without assuming that the movement is periodic. The goal of this

University of Utah. Lukas Gabert and Tommaso Lenzi are also affiliated with the Rocky Mountain Center for Occupational and Environmental Health. Tommaso Lenzi is also affiliated with the Department of Biomedical Engineering at the University of Utah (Corresponding author: Liam M. Sullivan, email: l.sullivan@utah.edu).

paper is to validate the proposed controller in one individual with an above-knee amputation walking at different speeds, different inclines, and on rough terrain, using a powered knee and ankle prosthesis.

#### II. METHODS

#### A. Controller

The proposed controller uses dedicated control methods for the knee and ankle modules during stance (foot on the ground) and swing (foot off the ground). A finite-state machine switches from stance to swing when the vertical ground reaction force (GRF) measures below 40 N (6% of user weight), and swing to stance when the GRF measures above 120 N (18% of user weight) (Fig. 1).

During stance, we determine the desired knee torque as the sum of two components: a virtual damping torque and a virtual biarticular torque ( $T_{Biart}$ ) as shown in (1).

$$T_{Knee} = -B_{Knee} \cdot \dot{\theta}_{Knee} + T_{Biart} \tag{1}$$

The virtual damping torque is proportional and opposite to the prosthesis knee velocity. Different damping coefficient values are used for extension  $(\dot{\theta}_{Knee} < 0)$  and flexion  $(\dot{\theta}_{Knee} > 0)$ , as shown in (2).

$$B_{Knee} = \begin{cases} B_{Ext}(\theta_{Knee}), & \text{if } \dot{\theta}_{Knee} < 0 \\ B_{Flex}(\theta_{Thigh}), & \text{if } \dot{\theta}_{Knee} > 0 \end{cases}$$
 (2)

The extension damping coefficient  $(B_{Ext})$  changes with prosthesis knee position (Fig. 2(a)) to slow the knee joint as it approaches full extension.  $B_{Ext}$  is zero when the knee position is flexed more than 20°. As the knee extends from 20° to 10°,  $B_{Ext}$  increases linearly until it reaches a maximum value of 0.1 Nm/kg. The flexion damping coefficient ( $B_{Flex}$ ) depends on the global orientation of the residual thigh  $(\theta_{Thigh})$ , which is negative when the thigh is anterior and positive when posterior.  $B_{Flex}$  is at its maximum value of 0.3 Nm/kg when the prosthesis is in front of the user ( $\theta_{Thigh} < 0$ ), preventing the knee from collapsing in early stance and mid-stance (Fig. 2(b)). Thigh angle increases as the residual thigh moves posteriorly and  $B_{Flex}$  decreases linearly to 0 between 5° and 10°. This allows the prosthetic knee joint to flex and initiate swing in late stance. The second component of the desired knee torque in stance is the virtual biarticular torque ( $T_{Biart}$ ).  $T_{Biart}$  provides knee flexion torque that increases with ankle plantarflexion torque, as shown in (3).  $T_{Biart}$  imitates the function of the gastrocnemius muscle, which flexes the knee when the ankle plantarflexes.

$$T_{Biart} = -K_{Biart}(\theta_{knee}) \cdot T_{AnkleFlex} \tag{3}$$

The biarticular gain ( $K_{Biart}$ ) depends on the position of the knee ( $\theta_{knee}$ ) (Fig. 2(c)).  $K_{Biart}$  is at its maximum value of 0.5

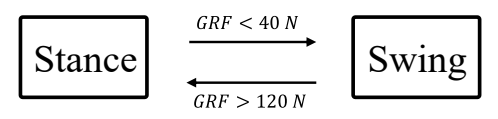


Fig. 1 High level control algorithm for stance and swing controller selection based on ground reaction force.

when the knee is flexed less than  $20^{\circ}$ .  $K_{\text{Biart}}$  decreases linearly to 0 from  $20^{\circ}$  to  $30^{\circ}$  of flexion. This position-dependent gain limits the biarticular flexion torque in late stance, preventing excessive knee flexion.

In stance, we define the desired ankle torque using an impedance-inspired controller as shown in (4).

$$T_{Ankle} = T_{Shank} + T_B \tag{4}$$

The first term in the ankle torque equation (4) is shank torque  $(T_{Shank})$ .  $T_{Shank}$  defines a desired ankle torque proportional to the (negated) global orientation of the shank  $(\theta_{shank})$  as shown in (5).  $\theta_{shank}$  is negative when anterior and positive when posterior.

$$T_{Shank} = K_{Shank} \cdot (0 - \theta_{Shank}) = -K_{Shank} \cdot \theta_{Shank}$$
 (5)

 $T_{Shank}$  is equivalent to creating a virtual ankle stiffness in which the deformation is equivalent to the difference between the gravity vector (i.e., 0°), which works as an equilibrium angle, and the  $\theta_{shank}$  (Fig. 2(d)). Therefore,  $T_{shank}$  pushes the shank back to a vertical position regardless of the ankle position. This virtual stiffness increases with the absolute value of  $\theta_{shank}$ , replicating the trend of ankle stiffness observed in non-amputee individuals [16].

The second term in the ankle torque equation (4) is a virtual damping torque (6-7) (Fig. 2 (e-f)).

$$T_B = -B_{Ankle} \cdot \dot{\theta}_{Ankle} \tag{6}$$

$$B_{Ankle} = \begin{cases} B_{DF}(v_{Hip}), & \text{if } \dot{\theta}_{Ankle} < 0 \\ B_{PF}(v_{Hip}), & \text{if } \dot{\theta}_{Ankle} > 0 \end{cases}$$
 (7)

Both dorsiflexion damping  $(B_{DF})$  and plantarflexion damping  $(B_{PF})$  depend on an online estimate of the walking speed,  $v_{hip}$  (Fig. 3). As walking speed increases, we decrease the magnitude of both  $B_{PF}$  and  $B_{DF}$  from maximum values of 1.3 and 1.2 Nm/kg, respectively, to 0. Decreased ankle damping results in less plantarflexion torque during dorsiflexion (early

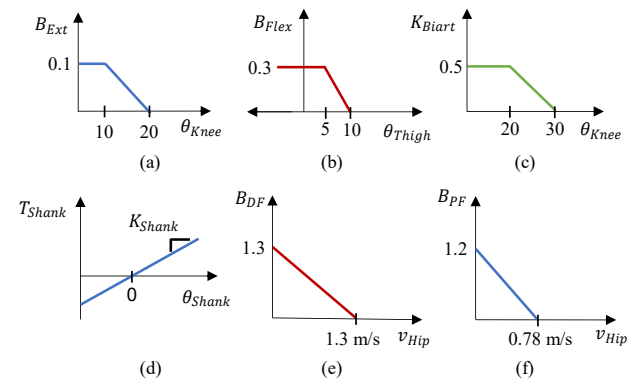


Fig. 2 Stance knee and ankle control relationships. (a) Extension knee damping coefficient relationship with knee angle. (b) Flexion knee damping coefficient relationship with thigh angle. (c) Biarticular knee torque gain as a function of knee angle. (d) Ankle virtual stiffness torque as a function of joint angle, equilibrium angle, and gain. (e) Ankle damping relationship in dorsiflexion (DF) ( $\dot{\theta}_{Ankle} < 0$ ) as a function of hip velocity. (f) Ankle damping relationship in plantarflexion (PF) ( $\dot{\theta}_{Ankle} > 0$ ) as a function of hip velocity.

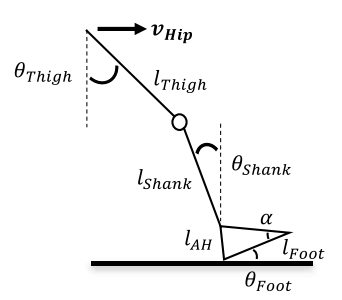


Fig. 3 Kinematic model of leg joint angles and segment lengths used to calculate horizontal hip velocity.

and mid-stance) and more plantarflexion torque during plantarflexion (late stance). The net result is more energy injected by the powered ankle during stance when walking speed increases, similar to non-amputee subject behavior [17]. Notably, both the plantarflexion and the dorsiflexion damping torques saturate at 0 N.

We use the hip's horizontal velocity  $(v_{Hip})$  as an approximation of walking speed in stance.  $v_{Hip}$  comes from a trigonometric equation based on the joint positions and velocities (Fig. 3) as shown in (8).

$$v_{Hip} = (\sin(\alpha + \theta_{Foot}) \cdot l_{Foot} \cdot \dot{\theta}_{Foot}) + (\cos(\theta_{Shank}) \cdot l_{Shank} \cdot \dot{\theta}_{Shank}) + (\cos(\theta_{Thigh}) \cdot l_{Thigh} \cdot \dot{\theta}_{Thigh})$$
(8)

During swing, we define the desired positions of the knee and ankle joints using a minimum-jerk optimizer [10]. The minimum-jerk optimizer creates an optimally smooth position trajectory based on the position and velocity of the prosthetic joints at the transition between stance and swing (Fig. 4), imitating able-bodied movements [18]. In the proposed controller, the end knee position of a swing trajectory is always zero. However, the desired swing duration is adapted online when the controller transitions from stance to swing based on the position of the ankle at the transition (Fig. 4). This approach is inspired by human biomechanics. As walking speed increases, cadence increases, reducing swing duration. Also, as walking speed increases the ankle position at the transition between stance and swing increases. The relationship between ankle joint position at the stance to swing transition and the subsequent swing duration is represented in our controller with (9).

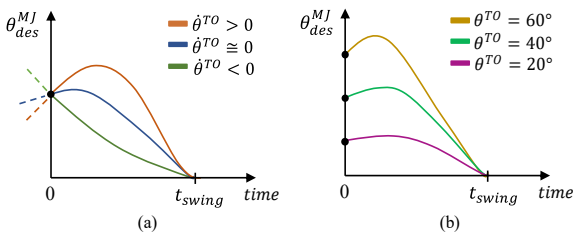


Fig. 4 Minimum jerk trajectory planning creates a smooth swing profile based on joint position and velocity at the stance to swing transition (TO), ending at a set swing time calculated by the ankle position at TO [10]. (a) Swing trajectories at positive, zero, and negative joint velocities at the transition to swing phase. (b) Swing trajectories at equal joint velocities but differing ankle toe-off angles at the transition to swing phase.

$$T_{swing} = K_{Swing} \cdot \theta_{Ankle}^{TO} \tag{9}$$

#### B. Hardware

In this study, we used the Utah Bionic Leg, a selfcontained, battery-operated, lightweight robotic prosthesis [5]. The Utah Bionic Leg consists of independent knee and ankle/foot modules capable of replicating the key biomechanical functions of the biological knee, ankle, and toe during ambulation. The powered knee module uses a torquesensitive actuator [19]. The powered ankle/foot module has two articulated joints, an ankle and a toe, which are powered by a single actuator using a compliant underactuated mechanism [20]. A custom instrumented pyramid adapter is located at the top of the ankle module to estimate the vertical ground reaction force (GRF) and torque in the sagittal plane [21]. The knee and ankle/foot modules are mechanically connected with a standard prosthetic pylon, which is cut to size for each user, as in commercially available prostheses. Combined, the powered knee and ankle/foot modules weigh 3.2 kg including batteries and protective covers.

# C. Experimental Protocol and Data Analysis

For this study, we recruited one subject with an above-knee amputation (30 years old, 65 kg, 178 cm, 9 years post-amputation). The subject is a full community ambulator (K3 classification) and uses the Freedom Plie Knee with an AllPro foot. The subject had prior experience with this powered prosthesis through participation in other studies. The Institutional Review Board at the University of Utah approved the study protocol. The subject provided informed consent to participate in the study and for the publication of photos and videos from the experiment.

A certified prosthetist fit and aligned the prosthesis prior to the experiment. After a short period of unstructured familiarization time, the subject walked on a level treadmill at 0.72 m/s, 1 m/s, and 1.25 m/s for 60 seconds each after reaching steady state speed. Next, they walked on a treadmill at 1 m/s on inclines of 0%, 5%, and 10% grade (0°, 2.86°, and 5.71°) for 60 seconds each after reaching steady state speed at each incline. Finally, they performed 10 trials of walking on rough terrain, in which they stepped once on level ground and then stepped twice with their prosthesis on a Sensa semi-rigid terrain patch Sensa (Ottobock, Item #: 752T1). We chose these trial lengths to capture enough strides to account for normal gait variability, while minimizing any concerns with the subject getting tired during the test. As an extra safety precaution, we asked the subject to rest their hands on the handrails whenever possible.



Fig. 5 Side view of participant wearing the Utah Bionic Leg during the experiment.

Kinematics and GRF data were recorded at 500 Hz by sensors embedded in the prosthesis. Data was processed offline in MATLAB. First, we segmented each stride from prosthesis heel strike to prosthesis heel strike, using the GRF readings. Then we interpolated each stride to 1,000 samples and computed average joint trajectories for each tested condition separately. Power was calculated as joint velocity multiplied by torque supplied by the motor. Energy injection per stride was calculated as the integral of the joint power over time during stance. Stride, stance, and swing durations were calculated using GRF readings. We analyzed the kinematic data to find the maximum and minimum knee and ankle joint angles, as well as the position of the ankle joint when the shank reached vertical angle ( $\theta_{Shank} = 0$ ).

#### III. RESULTS

# A. Variable Speed

The proposed controller automatically adapted the behavior of the powered prosthesis during stance and swing when the subject walked at different speeds (Fig. 6). Stride duration decreased with walking speed, averaging  $1.74 \pm 0.03$ s,  $1.47 \pm 0.03$  s, and  $1.30 \pm 0.02$  s, for 0.72 m/s, 1.0 m/s, and 1.25 m/s, respectively. Moreover, as the walking speed increased, the ankle position at toe off (colored dots, Fig. 6(a)) also increased, resulting in decreased swing durations of 0.60  $\pm 0.02$  s to  $0.55 \pm 0.03$  s to  $0.51 \pm 0.01$  s for 0.72 m/s, 1.0 m/s, and 1.25 m/s, respectively. Peak ankle angles increased at each speed, ranging from  $5.7 \pm 0.4^{\circ}$  to  $10.4 \pm 1.6^{\circ}$  to  $16.7 \pm$  $0.5^{\circ}$  in plantarflexion and  $-10.5 \pm 0.2^{\circ}$  to  $-11.9 \pm 0.7^{\circ}$  to -15.1 $\pm$  0.4° in dorsiflexion for 0.72 m/s, 1.0 m/s, and 1.25 m/s, respectively. These peaks were reached at around the same point in stride regardless of speed, at an average of  $64 \pm 1\%$ of stride for plantarflexion and  $45 \pm 2\%$  for dorsiflexion. Toeoff occurred at  $63 \pm 2\%$  of stride across speeds. Peak knee angles varied minimally across the three speeds, at  $69 \pm 2^{\circ}$ ,  $69 \pm 3^{\circ}$ , and  $71 \pm 1^{\circ}$ .

Finally, energy injected increased with each walking speed, from  $0.089 \pm 0.005$  J/kg to  $0.14 \pm 0.03$  J/kg to  $0.16 \pm 0.04$  J/kg at 0.72 m/s, 1.0 m/s, and 1.25 m/s, respectively. The slope of

the line-of-best-fit for these values is 0.14, similar to an ablebodied reference data fit of 0.26 [17].

#### B. Variable Incline

The proposed controller automatically adapted to different treadmill inclines (Fig. 7). There was little variation in the maximum ankle plantarflexion angle, which was  $11.3 \pm 0.7^{\circ}$ ,  $12.1 \pm 1.4^{\circ}$ , and  $11.3 \pm 2.1^{\circ}$ , for 0%, 5%, and 10% grade, respectively, occurring at  $65.6 \pm 1.6\%$  of stride across grades. In contrast, the peak ankle dorsiflexion angle changed visibly. reaching  $-11.4 \pm 0.3^{\circ}$ ,  $-15.7 \pm 0.5^{\circ}$ , and  $-18.6 \pm 0.5^{\circ}$ , for 0%, 5%, and 10% grade, respectively, and occurring at  $47 \pm 2\%$ of stride across grades. Knee position did not vary substantially, with maximum positions of  $66 \pm 3^{\circ}$ ,  $72 \pm 2^{\circ}$ and  $73 \pm 2^{\circ}$ , for 0%, 5%, and 10% grade, respectively, and occurring at  $72 \pm 1\%$  of stride across grades. Notably, there was no early stance knee flexion, a key characteristic of nonamputee gait. This result is likely due to the user exaggerating hip extension after heel strike, which is a common compensatory movement used by above-knee amputees to lock the prosthetic knee in extension and avoid knee buckling when they walk with their prescribed passive prostheses. Ankle energy increased visibly with the treadmill incline (Fig. 7 (b)). At 0%, 5%, and 10% grades, the ankle energy was  $0.03 \pm 0.05$  J/kg,  $0.09 \pm 0.08$  J/kg, and  $0.14 \pm 0.02$ J/kg, respectively. The slope of the line-of-best-fit to these energies is 0.011, closely matching the able-bodied reference trend of 0.013 [22]. When the shank was vertical with respect to gravity ( $\theta_{shank} = 0$ ), the angle of the ankle was  $3.8 \pm 0.3\%$ ,  $8.7 \pm 0.3\%$ , and  $14.1 \pm 0.5\%$  at the 0%, 5%, and 10% grade, respectively. The slope of the line-of-best-fit for the ankle angles at shank vertical is 1.03, showing the ability of the proposed controller to match the treadmill incline.

### C. Rough Terrain

The variability of the ankle joint trajectory was substantially higher when walking on rough terrains than on flat ground (Fig. 8(a)). Specifically, during stance, the average of the standard deviation of the ankle position across all strides on rough terrain was 7.3°, while the knee and shank positions had

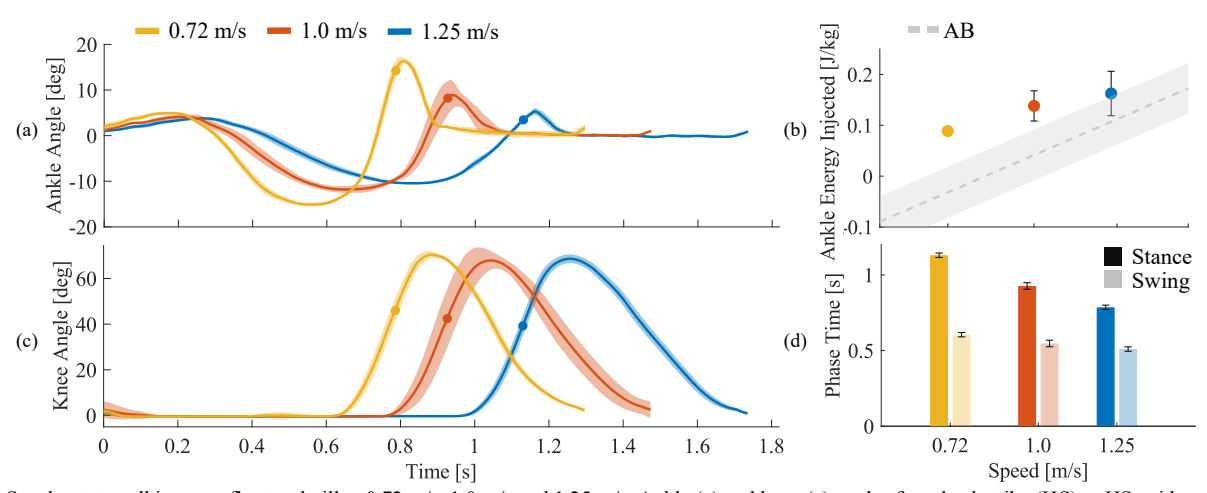


Fig. 6 Steady state walking on a flat treadmill at 0.72 m/s, 1.0 m/s and 1.25 m/s. Ankle (a) and knee (c) angles from heel strike (HS) to HS, with a solid line representing average values and shaded region representing one standard deviation above and below the average values. Solid dots indicate stance to swing TO point. (b) Energy injected by the ankle during stance phase, with solid dots representing average energy injection, error bars representing  $\pm$  one standard deviation, and the gray dashed line and shaded region representing able-bodied energy values [17]. (d) Stance (solid) and swing (transparent) phase times of stride at each speed, with error bars representing  $\pm$  one standard deviation.

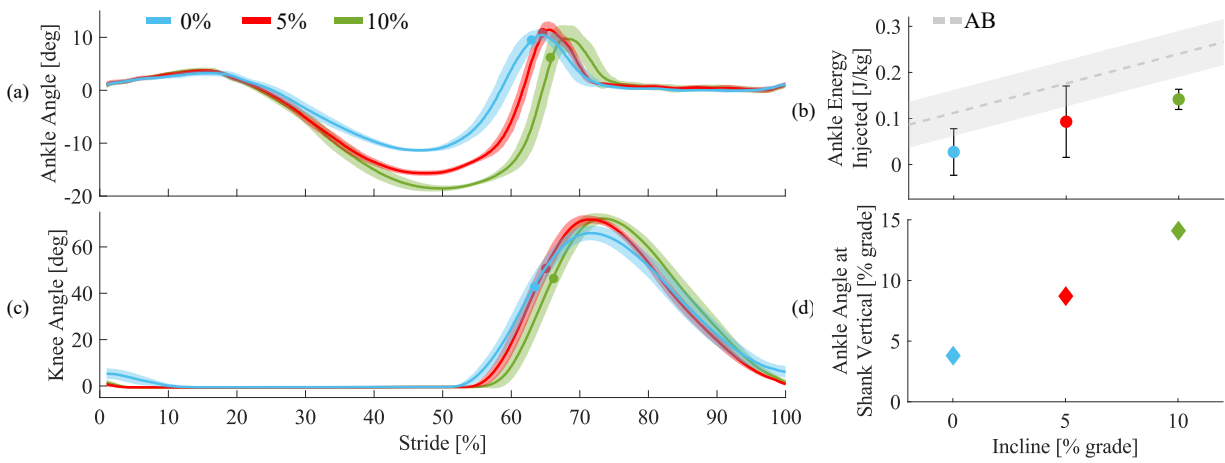


Fig. 7 Steady-state walking at 1.0 m/s and inclines of 0%, 5%, and 10% grade. Ankle (a) and knee (c) angles from heel strike (HS) to HS, with a solid line representing average values and shaded region representing one standard deviation above and below the average values. Solid dots indicate stance to swing TO point. (b) Energy injected by the ankle during stance phase, with solid dots representing average energy injection, error bars representing ± one standard deviation, and the gray dashed line and shaded region representing able-bodied energy values [22]. (d) Angle of the ankle when the shank reaches vertical during midstance phase of stride. Error bars indicating ± one standard deviation are hidden behind markers.

an average standard deviation of 0.6° and 3.5°, respectively (Fig. 8(d)).

Comparatively, during stance in flat ground walking, the average standard deviations of the ankle, knee, and shank position were 1.0°, 0.2°, and 2.2°, respectively. The difference between flat ground and rough terrain average standard deviation of positions was 6.3° for the ankle, 0.4° for the knee, and 1.3° for the shank.

#### IV. DISCUSSION

#### A. Significance

Seamless adaptation to different walking speeds, cadences, ground inclinations and terrain roughness is necessary for powered prostheses to work in the real world. In this paper, we show a control approach that enables continuous and automatic adaptation to walking speed, incline, and terrain without imposing a predefined trajectory. The proposed controller is inspired by invariant characteristics of non-amputee gait, such as shank-based impedance, biarticular muscle function, and minimum-jerk movements. The controller parameters were initially set to match nonamputee biomechanics in simulation and later refined through pilot experiments with amputee subjects. Our experimental data from one individual with an above-knee amputation suggests that the proposed controller can effectively adapt to different walking speeds, inclines, and rough terrains.

Adaptation to different walking speeds requires modulating the energy injected by the powered prosthesis into the gait cycle at the ankle joint. The proposed controller modulates this ankle energy by varying the ankle damping based on an online estimate of walking speed. The specific relationship between ankle damping and walking speed used in this experiment was originally determined while non-amputee subjects walked on the prosthesis using a bypass adapter and refined through experiments with amputee subjects. The ankle energy for this amputee participant follows the trend measured in non-amputee subjects [17], although the prosthetic ankle energy was slightly higher than the non-amputee reference to better match subject preference (Fig. 6(b)).

Adaptation to different walking speeds also requires changing the duration of swing. The proposed controller changes the swing duration based on the ankle angle at toe off. The greater the ankle angle at toe off, the faster the swing. This relationship provided similar results to our previous work, in which we used stance time to modulate swing [10]. However, this controller removes the assumption that the ambulation task is periodic, which may lead to better behavior

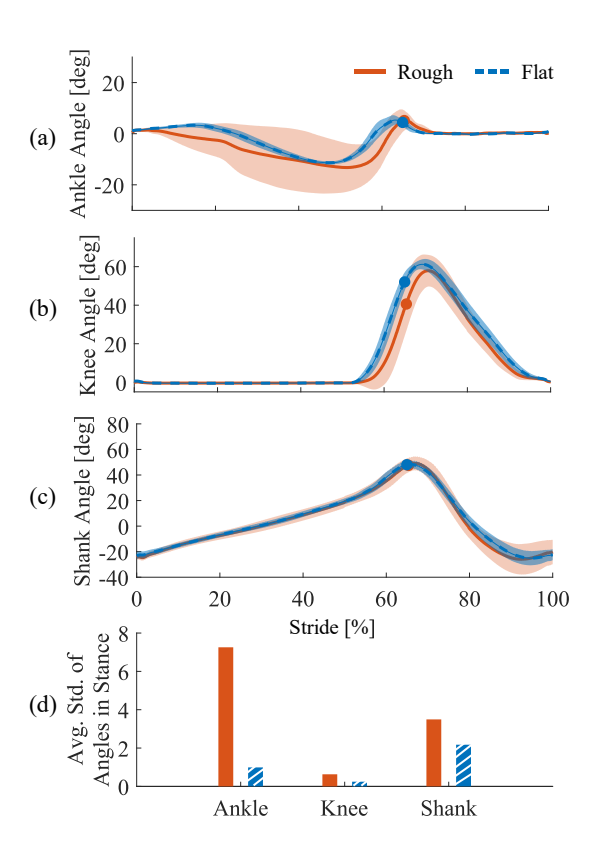


Fig. 8 Rough and flat ground walking. Ankle (a), knee (b), and shank (c) angle from HS to HS, with solid lines representing average values and shaded regions representing one standard deviation above and below the average values. (d) The average standard deviation of angles in stance, representing the average of the standard deviations in the plots above.

for non-steady-state gait including starting and stopping, turning, and cutting.

Walking at variable inclines and on rough terrains requires rapid adaptation of the foot orientation to match the ground in mid-stance, when the shank is roughly vertical. The proposed controller uses the global orientation of the shank to define the ankle torque across inclines. A similar approach was previously used in a powered ankle prosthesis for a belowknee amputee [15]. However, the previous study only used the shank angle to adapt to the ground in mid-stance and not to modulate the ankle push off behavior. Our study contributes to the field by showing that shank-based ankle impedance can provide both ground adaptation and energy modulation. Our results show that shank-based impedance control leads to biomimetic ankle energy increases with increasing ground inclinations. Moreover, we show for the first time that this adaptation mechanism can be used in powered knee and ankle prostheses for above-knee amputees.

#### B. Limitations

This study has several limitations. The most significant is that we only recruited one amputee subject. Therefore, we do not know if the controller can generalize to other individuals. Additionally, we only tested three different speeds and three different treadmill inclines. Although the behavior of the controller is continuous by design, we do not know how the controller will behave when the speed and incline changes continuously. We also do not know how the controller behaves at speeds and inclines that were not tested. Finally, we did not test the ability of the controller to adapt to the needs and subjective preference of the user. The behavior of the powered prosthesis is determined by a few key parameters. For example, the adaptation to different inclines and rough terrains could be changed by altering the stiffness of the shank impedance. Energy injected by the powered ankle at different walking speeds may be changed by altering the ankle damping, and cadence could be changed by altering the relationship between the ankle position and the swing duration. We did not perform tests altering these components. Therefore, although the proposed controller does not enforce non-amputee prosthesis trajectories, we do not know whether it can be personalized to each subject.

## V.CONCLUSION

This study presents a powered prosthesis controller that continuously and automatically adapts to different walking speeds, inclines, and rough terrain without enforcing non-amputee impedance or position trajectories. Future work should focus on testing with a broader population, more speeds, and more inclines to assess the generalization and personalization capabilities of the proposed controller.

#### REFERENCES

- [1] T. Schmalz, S. Blumentritt, and R. Jarasch, "Energy expenditure and biomechanical characteristics of lower limb amputee gait: The influence of prosthetic alignment and different prosthetic components." [Online]. Available: www.elsevier.com/locate/gaitpost
- [2] B. E. Lawson, J. Mitchell, D. Truex, A. Shultz, E. Ledoux, and M. Goldfarb, "A Robotic Leg Prosthesis: Design, Control, and Implementation," *IEEE Robot Autom Mag*, vol. 21, no. 4, pp. 70–81.
- [3] A. F. Azocar, L. M. Mooney, J.-F. Duval, A. M. Simon, L. J. Hargrove, and E. J. Rouse, "Design and clinical implementation of an open-source bionic leg," *Nat Biomed Eng*, vol. 4, no. 10, pp. 941–953, Oct. 2020.

- [4] T. Elery, S. Rezazadeh, C. Nesler, and R. D. Gregg, "Design and Validation of a Powered Knee–Ankle Prosthesis With High-Torque, Low-Impedance Actuators," *IEEE Transactions on Robotics*, vol. 36, no. 6, pp. 1649–1668, Dec. 2020.
- [5] M. Tran, L. Gabert, S. Hood, and T. Lenzi, "A lightweight robotic leg prosthesis replicating the biomechanics of the knee, ankle, and toe joint," *Sci Robot*, vol. 7, no. 72, Nov. 2022.
- [6] M. Tran, L. Gabert, M. Cempini, and T. Lenzi, "A Lightweight, Efficient Fully Powered Knee Prosthesis with Actively Variable Transmission," *IEEE Robot Autom Lett*, vol. 4, no. 2, pp. 1186–1193, Apr. 2019.
- [7] R. D. Gregg, T. Lenzi, L. J. Hargrove, and J. W. Sensinger, "Virtual Constraint Control of a Powered Prosthetic Leg: From Simulation to Experiments With Transfemoral Amputees," *IEEE Transactions on Robotics*, vol. 30, no. 6, pp. 1455–1471.
- [8] D. Quintero, D. J. Villarreal, D. J. Lambert, S. Kapp, and R. D. Gregg, "Continuous-Phase Control of a Powered Knee–Ankle Prosthesis: Amputee Experiments Across Speeds and Inclines," *IEEE Transactions on Robotics*, vol. 34, no. 3, pp. 686–701, Jun. 2018.
- [9] S. Rezazadeh, D. Quintero, N. Divekar, E. Reznick, L. Gray, and R. D. Gregg, "A Phase Variable Approach for Improved Rhythmic and Non-Rhythmic Control of a Powered Knee-Ankle Prosthesis," *IEEE Access*, vol. 7, pp. 109840–109855, 2019.
- [10] T. Lenzi, L. Hargrove, and J. Sensinger, "Speed-adaptation mechanism: Robotic prostheses can actively regulate joint torque," *IEEE Robot Autom Mag*, vol. 21, no. 4, pp. 94–107, Dec. 2014.
- [11] J. Mendez, S. Hood, A. Gunnel, and T. Lenzi, "Powered knee and ankle prosthesis with indirect volitional swing control enables level-ground walking and crossing over obstacles," *Sci Robot*, vol. 5, no. 44, Jul. 2020.
- [12] A. M. Simon et al., "Configuring a Powered Knee and Ankle Prosthesis for Transfemoral Amputees within Five Specific Ambulation Modes," PLoS One, vol. 9, no. 6, p. e99387, Jun. 2014.
- [13] F. Sup, H. A. Varol, and M. Goldfarb, "Upslope Walking With a Powered Knee and Ankle Prosthesis: Initial Results With an Amputee Subject," *IEEE Transactions on Neural Systems and Rehabilitation Engineering*, vol. 19, no. 1, pp. 71–78, Feb. 2011.
- [14] T. K. Best, C. G. Welker, E. J. Rouse, and R. D. Gregg, "Data-Driven Variable Impedance Control of a Powered Knee–Ankle Prosthesis for Adaptive Speed and Incline Walking," *IEEE Transactions on Robotics*, pp. 1–19, 2023.
- [15] A. H. Shultz, B. E. Lawson, and M. Goldfarb, "Variable Cadence Walking and Ground Adaptive Standing With a Powered Ankle Prosthesis," *IEEE Transactions on Neural Systems and Rehabilitation Engineering*, vol. 24, no. 4, pp. 495–505, Apr. 2016, doi: 10.1109/TNSRE.2015.2428196.
- [16] K. Shamaei, G. S. Sawicki, and A. M. Dollar, "Estimation of Quasi-Stiffness and Propulsive Work of the Human Ankle in the Stance Phase of Walking," *PLoS One*, vol. 8, no. 3, p. e59935, Mar. 2013.
- [17] M. L. Palmer, "Sagittal plane characterization of normal human ankle function across a range of walking gait speeds," *Massachusetts Institute* of *Technology*, 2002.
- [18] Q.-C. Pham, H. Hicheur, G. Arechavaleta, J.-P. Laumond, and A. Berthoz, "The formation of trajectories during goal-oriented locomotion in humans. II. A maximum smoothness model," *European Journal of Neuroscience*, vol. 26, no. 8, pp. 2391–2403, Oct. 2007.
- [19] M. Tran, L. Gabert, and T. Lenzi, "Analysis and Validation of Sensitivity in Torque-Sensitive Actuators," *Actuators*, vol. 12, no. 2, p. 80, Feb. 2023.
- [20] L. Gabert, M. Tran, and T. Lenzi, "Design of an Underactuated Powered Ankle and Toe Prosthesis," in 2021 43rd Annual International Conference of the IEEE Engineering in Medicine & Biology Society (EMBC), IEEE, Nov. 2021, pp. 4920–4923.
- [21] L. Gabert and T. Lenzi, "Instrumented Pyramid Adapter for Amputee Gait Analysis and Powered Prosthesis Control," *IEEE Sens J*, vol. 19, no. 18, pp. 8272–8282, Sep. 2019.
- [22] A. N. Lay, C. J. Hass, and R. J. Gregor, "The effects of sloped surfaces on locomotion: A kinematic and kinetic analysis," *J Biomech*, vol. 39, no. 9, pp. 1621–1628, 2006.